IV International Conference on Computational Methods for Coupled Problems in Science and Engineering
COUPLED PROBLEMS 2011
M. Papadrakakis, E. Oñate and B. Schrefler (Eds)

DYNAMIC BEHAVIOUR OF SATURATED POROELASTIC LAYERS WITH EMBEDDED WALL SUBMITED TO SEISMIC ACTIONS

GRAZINA, J. C.* AND PINTO, P. L.†

Dep. Engenharia Civil – Fac. Ciências e Tecnologia da Universidade de Coimbra (FCTUC)
Universidade de Coimbra
Polo II, 3030-788 Coimbra, Portugal
*e-mail: graza@dec.uc.pt
†e-mail: ppinto@dec.uc.pt

Key words: Soil-structure interaction, Finite elements model, Poroelastic saturated materials, Time domain analysis, Viscous damping.

Summary. Behaviour of poroelastic saturated materials submitted to dynamic actions is strongly dependent of the solid skeleton permeability and the frequency of the movement. Depending on these quantities, undrained behaviour or fully drained behaviour occurs for total coupled interaction or for null interaction, respectively. Between these limit cases, some relative movement occurs among solid skeleton and fluid, generating viscous damping, which, in turn, modifies the elastic response of the system. This paper presents results of coupled behaviour in poroelastic saturated layers with an embedded impermeable wall, submitted to seismic actions. A Finite Element code developed at the University of Coimbra (FEMEPDYN), with coupled formulation u^s–u^w–p, was used for this purpose. Dynamic responses of poroelastic layers with an embedded wall are compared with non-porous materials for similar conditions. Damping of non-porous materials was previously calculated by calibration of the Rayleigh coefficients in order to match the free field responses for both materials types. Unlike for the free field analysis, results reveal some differences between both materials responses with the presence of the wall, due to the volumetric deformations imposed by the embedded wall. Also, those volumetric deformations have a more uniform distribution in poroelastic layers with permeabilities that represent near total and near fully drained behaviour.

1 INTRODUCTION

Behaviour of poroelastic saturated materials is actually described using two theories: the Biot theory [1, 2], based on the Lagrange classical mechanics, and the Porous Mixtures theory, firstly presented by Fillunger (1913), which involves the concept of volume fractions [3]. Considering some simplifications and the incompressibility of the constituents, both theories result in similar coupled equilibrium equations, where the interaction force between porous solid skeleton and the interstitial fluid is expressed by:

$$R = \frac{n^2 \gamma_w}{k} (v^w - v^s) \quad (1)$$

where k is the permeability, n is the porosity, γ_w is the bulk unit weight of fluid, v^s is the velocity of solid and v^w is the velocity of fluid.

Interaction forces between the solid skeleton and the fluid in a poroelastic saturated material are greatly dependent on the permeability and frequency of the movement. Zienkiewicz et al. [4] presented parametric analyses for wide ranges of permeabilities and frequencies of harmonic vertical excitations in a poroelastic column. These authors found bound parameters related to the limit levels of coupled interaction, from near drained behaviour (quasi-null coupled interaction) to near undrained behaviour (quasi-total coupled interaction), for a range of loading velocities from the quasi-static (consolidation problem in despite to inertial forces) to the rapid loading. For near undrained behaviour, relative movements between solid and fluid are very small and viscous interaction forces developed are insignificant. In the opposite situation, for near full drained behaviour, permeabilities are very high and, consequently, viscous interaction forces are very small, in spite the existence of large relative movements between both phases. In between these limiting situations, relevant viscous interaction forces may be developed for common dynamic loadings, as those originated by foundations of industry equipment or earthquakes.

Viscous damping values due to coupled interaction forces were previously calculated on poroelastic saturated layers subjected to shear free field movements [5]. In these analyses, only shear deformations are induced and, consequently, excess pore pressures are inexistent. Permeabilities for near limit cases of coupled interaction with quasi-null damping were found, as well the damping ratios for middle range permeabilities. The absence of excess pore pressure generation allows the use of non-porous linear elastic materials for the calculations of the dynamic responses: with dry properties for quasi-null coupled interaction and with saturated undrained properties for quasi-total coupled interaction. In between these limit cases, appropriate Rayleigh damping can be used in non-porous materials for the same purpose [6]. Main advantages of the use of non-porous materials in finite elements models are the much lower effort and time computing.

Shear movements induced on saturated porous layers with embedded impermeable walls produce non-homogeneous fields of volumetric deformations and excess pore pressures generation. This factor influences the whole response of the layer and tends to disregard the previously related in free field conditions. Analyses are presented for an artificial seismic action applied at the base of the layers.

2 NUMERICAL MODELLING

2.1 Finite element code

The numerical analyses were carried using the finite element code FEMEPDYN [6], developed at the University of Coimbra. FEMEPDYN code uses the Generalized-α time integration algorithms to perform dynamic calculations in time domain, for both non-porous and porous materials. The porous materials are modelled by the u^s-u^w-p coupled formulation [7, 8]. At each time step this formulation enables the computation of nodal displacements, velocities and accelerations (d.v.a.) of both solid and fluid phases, as well pore pressures

(p.w.p.) at the corner nodes of the mesh elements. For this purpose, finite element meshes are composed by quadrangular hybrid elements with 8 nodes of Q8/C4 type, which ensures fluid pressure continuity between elements (Figure 1a). Meshes for non-porous materials are composed with isoparametric quadrangular elements of 8 nodes.

2.2 Materials properties

Properties of the poroelastic and non-porous materials are presented in Table 1 and Table 2, respectively. Shear modulus values of 20 MPa (G20) and 80 MPa (G80) were considered for both materials types. The pore fluid in the poroelastic analyses is almost incompressible, with a bulk modulus of K_w=1×10^8 MPa. The permeability coefficients adopted varies in a wide range with the purpose to achieve the two near limit cases of viscous interaction – for the quasi-null coupled behaviour unrealistic high permeability coefficients were used.

The reproductions of poroelastic behaviours were carried with two types of non-porous materials: for the drained behaviours and allowable volumetric deformations with the Poisson coefficient of the solid skeleton (ν=0.3); for the undrained behaviours with a Poisson coefficient of ν=0.49. Differences in results between these non-porous materials should not be detectable in movements without volumetric deformations, as occurs in pure shear column analyses. The bulk unit weights of non-porous materials were calculated using the solid skeleton and pore fluid densities of the poroelastic materials, respectively ρ_s and ρ_w. For movements caused by shear wave propagation, bulk unit weights should be calculated considering saturated and dry materials, respectively for undrained and drained conditions [9]. Densities of saturated and dry materials, ρ_{sat} and ρ_d, are calculated using Equations 2 and shear wave velocities, v_S, are calculated using Equation 3 for respective ρ value.

$$\text{Saturated:} \quad \rho = \rho_{sat} = (1-n)\rho_s + n\rho_w \tag{2}$$

$$\text{Dry:} \quad \rho = \rho_d = (1-n)\rho_s$$

$$v_S = \sqrt{\frac{G}{\rho}} \tag{3}$$

Table 1: Properties of poroelastic materials

G (MPa)	E_s (MPa)	ν	ρ_s (kg/m^3)	ρ_w (kg/m^3)	K_w (MPa)	n	k (m/s)
20	52	0.3	2.6×10^3	1.0×10^3	1×10^5	0.365	1×10^2 to 1×10^{-5}
80	208						

Table 2: Properties of non-porous materials

G (MPa)	E_s (MPa)	ν	Coupled interaction / Material	γ (kN/m^3)	v_S (m/s)
20	52.0	0.3	Null / Dry	16.20	110.1
	59.6	0.49	Total / Saturated	19.78	99.6
80	208.0	0.3	Null / Dry	16.20	220.1
	238.4	0.49	Total / Saturated	19.78	199.2

The embedded wall has a linear elastic behaviour and was considered as a non-porous material in all the analyses. The elastic properties are respective to a common concrete material, with an elasticity modulus of E=20 GPa and a Poisson coefficient of ν=0.2.

2.3 Models meshes

The modelled media consists in homogeneous layers with 20 m thickness, settled over a rigid and impervious bedrock material. The width of the FE domain depends of the analyses type: for the free field response of the layer, the existence of only pure shear horizontal movements allows the use of a single column; for the analyses with the embedded wall, a larger mesh of 50.4 m width is used in order to mitigate the influence of the lateral boundaries on wall movements. In both cases, the lateral boundaries have restrictions for vertical displacements and the bottom boundary is impervious and has vertical displacement restrictions. In free vibration analyses, the bottom boundary has also horizontal displacements restrictions. In other analyses, horizontal accelerations (harmonic or seismic) are imposed at the bottom boundary. The stiffness of layer is related with velocity of wave propagation (Eq. 3) and modal frequencies (Eq. 4). Higher values require more refined meshes in wave propagation direction to obtain accurate results. Therefore, for layers G20 and G80, 20 and 40 elements uniformly distributed in vertical direction were adopted in respective meshes.

In the FE models with embedded wall, interface joint elements with no thickness were inserted between wall and surrounding layer. Parameters of constitutive model of these joint elements were chosen with extremely low tangential stiffness and high normal stiffness. In these conditions, an almost free shear displacement is allowed and avoided the opening of gaps in the mesh. Formulation of these joint elements may consider both impervious or permeable interfaces. In the analyses here presented, permeable case is considered. The wall is 12 m deep and 0.4 m thick.

Figure 1 presents a scheme of the hybrid elements used in poroelastic analyses, the FE mesh column used in the free field analyses and the right half of the mesh used in the analyses with the embedded wall.

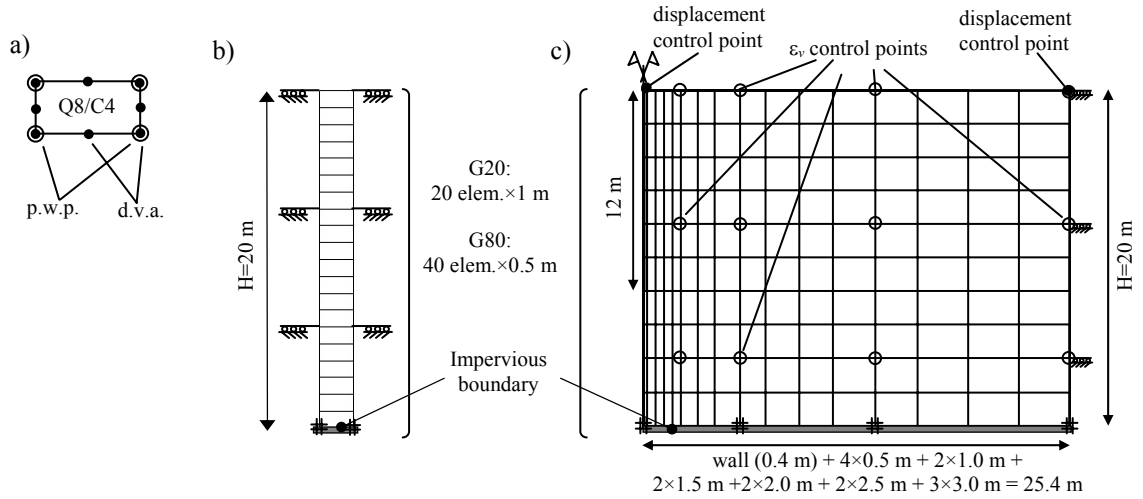

Figure 1: Finite element meshes: a) Hybrid elements; b) Free field; c) Layer with embedded wall.

2.4 Seismic action

The seismic action is an artificial accelerogram generated by the SeismoSignal software [10], so as to match an elastic response spectrum defined by the Eurocode 8 [11]. Parameters of this spectrum were chosen for the seismic zone of Coimbra (Portugal), a seismic action of Type 2 (lower magnitude and epicentre in continental territory) and for Ground Type A (bedrock layer, considering the seismic action applied at the rigid base boundary of the finite element mesh). Figure 2 presents the accelerogram adopted in the analyses with a time duration of 22 seconds, that includes a stationary part of 10 seconds, and a maximum ground acceleration of a_g=1.3 m/s^2. The time steps used are of 0.01 seconds for G20 layers and 0.005 seconds for G80 layers (regarding the higher frequencies existent in this layers movement).

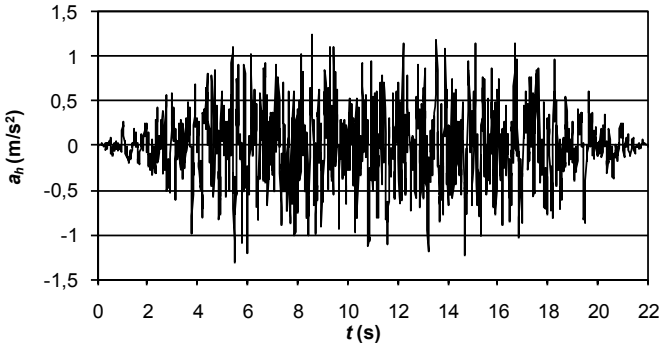

Figure 2: Artificial accelerogram used in the analyses

3 EVALUATION OF VISCOUS DAMPING IN FREE FIELD SHEAR MOVEMENT

3.1 Methodology

Here is presented a description of the method to evaluate the modal frequencies and respective damping ratio of poroelastic saturated layers in free field conditions. Analyses were made for the range of permeabilities presented in Table 1.

Firstly, a free vibration horizontal movement was induced at the layer by releasing a pre-imposed displacement on the top of the column. From the free vibration responses, modal frequencies were calculated using a Discrete Fourier Transformer (DFT) algorithm [12]. Secondly, harmonic shear accelerations, with the previously calculated modal frequencies, were imposed at the base of the layer exciting only one mode at once. The one-mode response tends to be infinitely amplified in the absence of viscous damping, as approximately occurs for permeability values near the limit cases of total and null coupled interaction. For middle range permeabilities, viscous damping restricts amplification of the movements and a steady state response is achieved. As an example, the amplified response for the 1st mode of the layer G20 with k=1×10^{-1} m/s is presented in Figure 3. The amplification value obtained, D, allows the calculation of the damping coefficient, ξ, for each vibration mode, using the simplified equation for homogeneous layers [13]:

$$D = \sinh\left((2n-1)\xi \frac{\pi}{2} \right)^{-1} \tag{4}$$

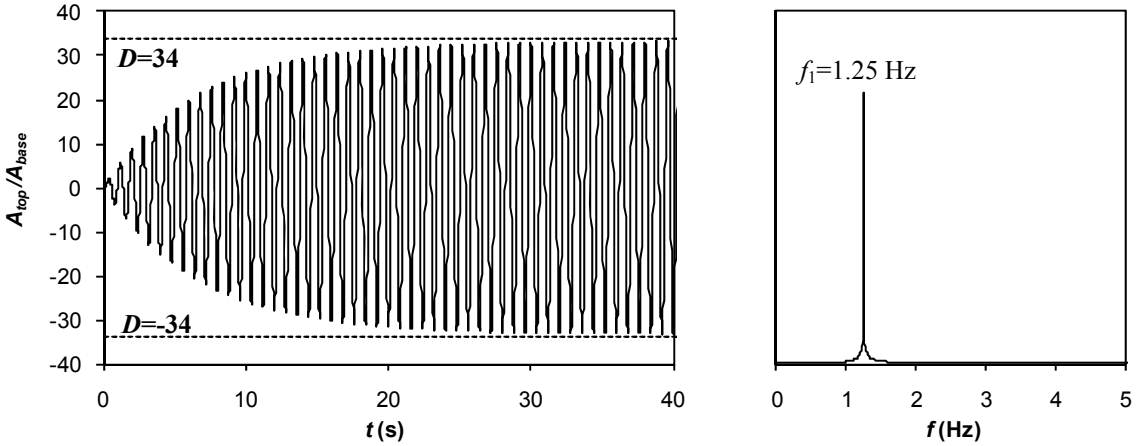

Figure 3: Amplified response and frequency spectra for harmonic action with 1st mode frequency.

3.2 Free vibration responses

The elastic deformations due to a pre-imposed displacement, d_0, on the top of the column, released at t=0s, induce a pure shear movement in free vibration mode. Depending on the coupled interaction between the fluid and solid skeleton, ruled by permeability, different levels of viscous damping are developed. In Figure 3 are presented the envelopes of the normalized displacements during the first 40 seconds of free vibration movement.

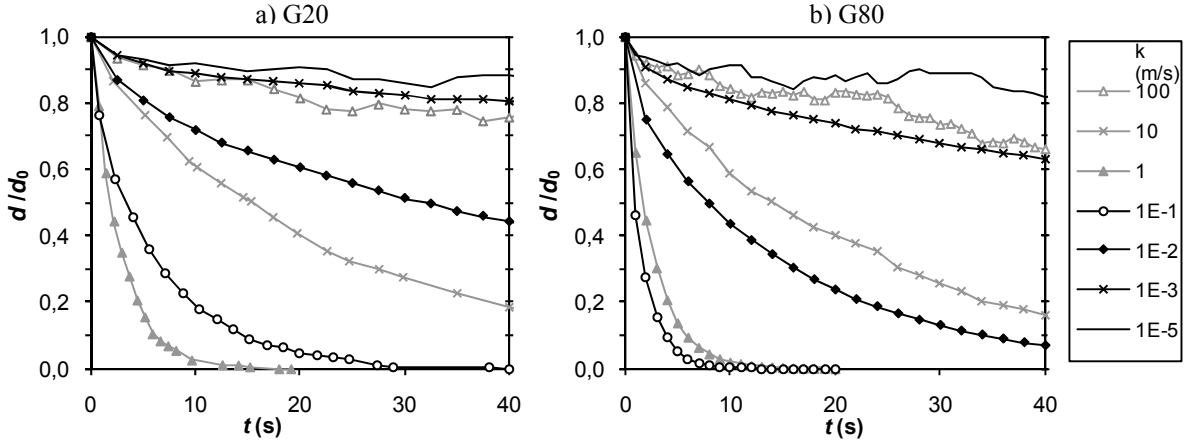

Figure 4: Time variation of displacement amplitudes in free vibration mode for several permeabilities.

The figures show a sharp decrease of displacement amplitudes with decreasing permeabilities from k=100m/s to 1m/s for G20 and to 0.1m/s for G80. For these last permeabilities a noticeable higher viscous damping is developed during the movement. For lower permeabilities, viscous damping tends to decrease as can be noticed by the less damped movements. Lower damping occurs for $k=1\times10^{-5}$m/s and k=100m/s, denoting their similitude of behaviour with the undamped coupled limit cases. Anyway, time decreasing amplitudes are noticeable for these higher and lower values of k, particularly for k=100m/s, which means that limit cases are not completely achieved and some residual damping is present.

3.3 Modal frequencies

Analytical value of the n modal frequency for homogeneous layers can be calculated with the well known expression:

$$f_n = (2n-1)\, v_S / 4H \tag{5}$$

where v_S is the shear wave velocity (Eq. 3), and H is the thickness of the layer.

The results of the 1st and 2nd modal frequencies detected from spectral distributions for the aforementioned free vibration responses, as well analytical values obtained from Equation 5, are compiled in Table 3. Cases where dispersive frequency distribution hinders the achievement of accurate frequency higher modes are also presented in brackets.

Analytical and calculated values for non-porous materials are in good agreement, which is a trustful indication that appropriate meshes and time steps had been used. This table shows that modal frequencies of poroelastic materials can be separated in two sets, each one with values similar to those of coupled limit cases calculated with non-porous materials. In each set, the pure shear behaviour of the poroelastic material can be reproduced using the respective non-porous material with an appropriate viscous damping. It is visible that the transition from dry to saturated behaviours occurs suddenly for permeabilities between k=1m/s to k=1×10^{-1}m/s, for both G20 and G80, when viscous damping effect is more notorious (as shown in Figure 4).

Table 3: Modal frequencies for different coupled interaction levels

Coupled interaction		G20		G80	
	Permeability	Modal frequencies		Modal frequencies	
	k (m/s)	f_1 (Hz)	f_2 (Hz)	f_1 (Hz)	f_2 (Hz)
Null / Analytical ($\rho=\rho_d$)	∞	1.376	4.127	2.752	8.255
Null / Non-porous ($\rho=\rho_d$)	∞	1.375	4.120	2.750	8.240
Poroelastic	100	1.375	4.120	2.750	8.240
	10	1.375	4.120	2.750	8.245
	1	1.350	4.125	2.740	8.240
	10^{-1}	1.250	(3.908)	2.540	(8.375)
	10^{-2}	1.245	(3.735)	2.490	(7.490)
	10^{-3}	1.245	3.730	2.490	(7.460)
	10^{-4}	1.245	3.730	2.490	7.460
	10^{-5}	1.245	3.730	2.490	7.460
Total / Analytical ($\rho=\rho_{sat}$)	0	1.245	3.735	2.490	7.470
Total / Non-porous ($\rho=\rho_{sat}$)	0	1.245	3.730	2.490	7.460

( ) Inaccurate values.

3.4 Viscous damping

The steady-state responses for harmonic actions with modal frequencies allow the calculation of damping ratios, ξ, of the first two modes for the middle range permeabilities. For the lowest and highest permeability values, the residual damping present is not enough to hinder an increasing amplification of the responses, therefore, to establish a ξ value. Also, determination of the ξ values for higher modes is defected of the indelible presence of the lower modes. Despite these limitations, values of ξ presented in Table 4 are in accordance with damped responses presented in Figure 3.

Table 4: Modal damping ratios for different coupled interaction levels

k (m/s)	G20 layer		G80 layer	
	ξ_1 (%)	ξ_2 (%)	ξ_1 (%)	ξ_2 (%)
100	<0.05	--	<0.05	--
10	0.45	0.18	0.23	(0.12)
1	3.74	1.51	2.16	0.76
10^{-1}	1.87	4.68	3.53	6.95
10^{-2}	0.21	--	0.40	1.18
10^{-3}	<0.05	--	<0.05	(0.14)

-- Not detectable values; ( ) Inaccurate values.

4 ANALYSES WITH THE SEISMIC ACTION

4.1 General description

The behaviours of poroelastic and non-porous layers are compared for equivalent viscous damping conditions. For that purpose, damping ratios previously obtained for poroelastic layers (Table 4) are considered for the calculation of Rayleigh damping parameters, a_0 and a_1 used in non-porous materials, These Rayleigh parameters are calculated for the modal frequencies f_1 and f_2 presented in limit coupled cases (Table 3). Limit case frequencies, and therefore dry or saturated non-porous properties, are chosen according to proximity of frequency values observed in poroelastic layer which is intended to be replicated. Table 5 presents the designations and main characteristics of the carried analyses with poroelastic and non-porous materials.

Table 4: Characteristics of the comparative analyses with seismic action.

G (MPa)	Poroelastic		Non-porous			
	Analysis	k (m/s)	Analysis	Coupled inter. / Material	Rayleigh coefficients	
					a_0	a_1
20	G20_k-5	10^{-5}	G20_sat	Total / Sat.	0	0
	G20_k-1	10^{-1}	G20_sat_R	Total / Sat.	0.05421	3.90×10^{-3}
	G20_k1	10	G20_dry_R	Null / Dry	0.07582	2.59×10^{-5}
80	G80_k-5	10^{-5}	G80_sat	Total / Sat.	0	0
	G80_k-1	10^{-1}	G80_sat_R	Total / Sat.	0.42616	2.77×10^{-3}
	G80_k1	10	G80_dry_R	Null / Dry	0.07387	1.88×10^{-5}

4.1 Responses of layers in free field conditions

The time variation of relative displacements on the top of the layers ($u'=u_{top}-u_{base}$) is presented in Figure 5, for the several analyses. In this figure a good match between displacements in poroelastic and non-porous layers is visible, meaning that poroelastic behaviour can be fairly reproduced with non-porous damped materials (or undamped materials for quasi-limit coupled cases), in pure shear conditions. Also frequency spectra (not shown here) are very similar for both materials in these studied cases. A large amplification of displacements is found for $k=1\times10^{-5}$m/s analyses, particularly visible for the G80 layer, due to the almost absence of viscous damping in these cases.

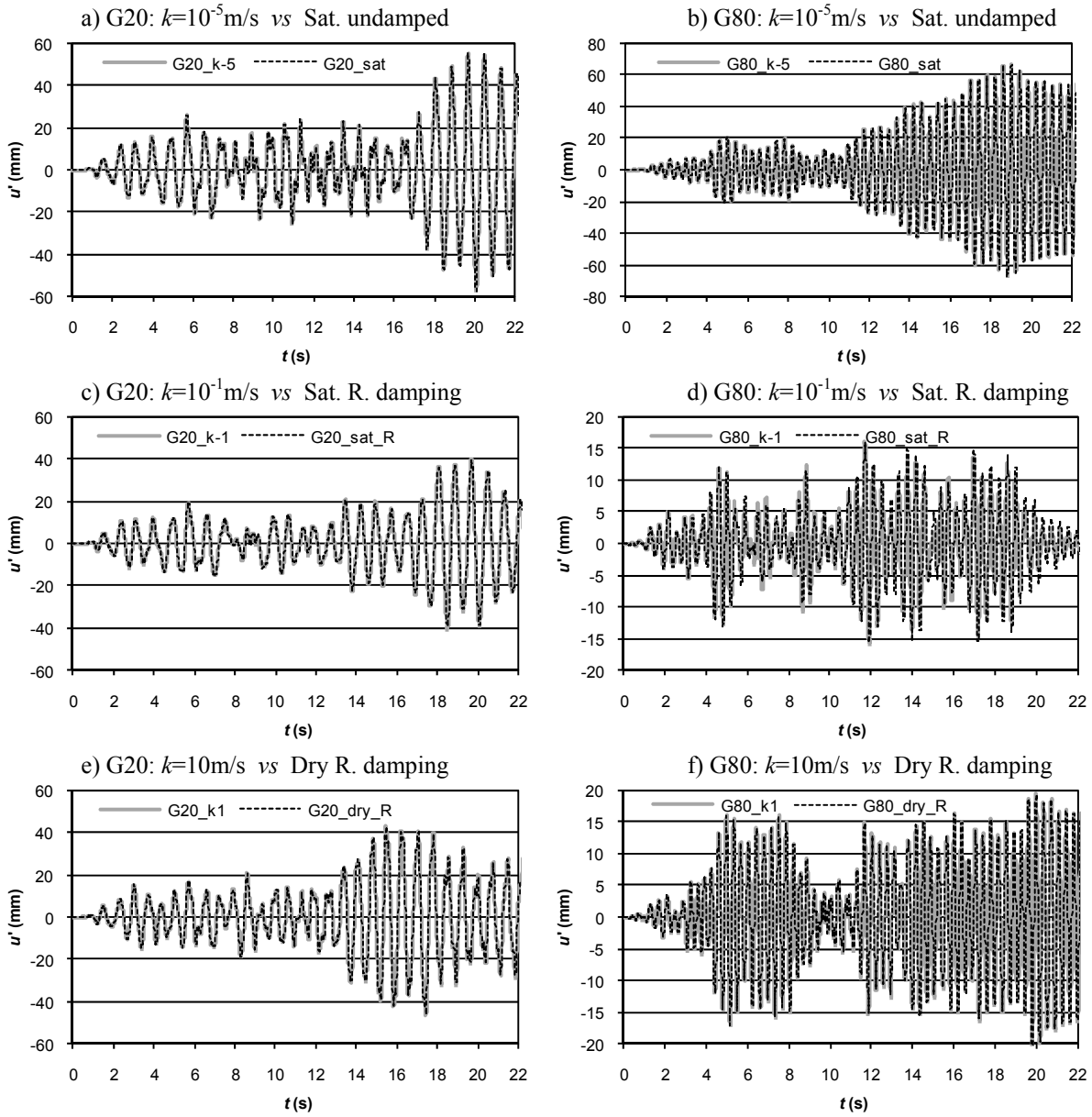

Figure 5: Time variation of displacement amplitudes in free vibration mode for several permeabilities.

4.2 Responses of layers with embedded wall

Some results of the above-mentioned analyses are presented in Figure 6. In this figure, comparisons of relative displacements between poroelastic and non-porous layers are displayed for the top of the layers, above the wall and on the boundary (displacement control points marked in Figure 1c). These results are in agreement with that observed in free field analyses, denoting a good, but not so perfect, match of displacements between both materials. In these figures a higher amplification of responses is observed on the top of the wall, enhanced particularly for the less damped materials as G80_k-5 and G20_k1.

Responses are less amplified at the boundaries, denoting a decreasing influence with the

distance of the wall. Anyway, the boundary displacements have some differences from those of the free field analyses, mainly for the less damped materials, which mean that these boundaries are not sufficiently far from the wall to reproduce the free field.

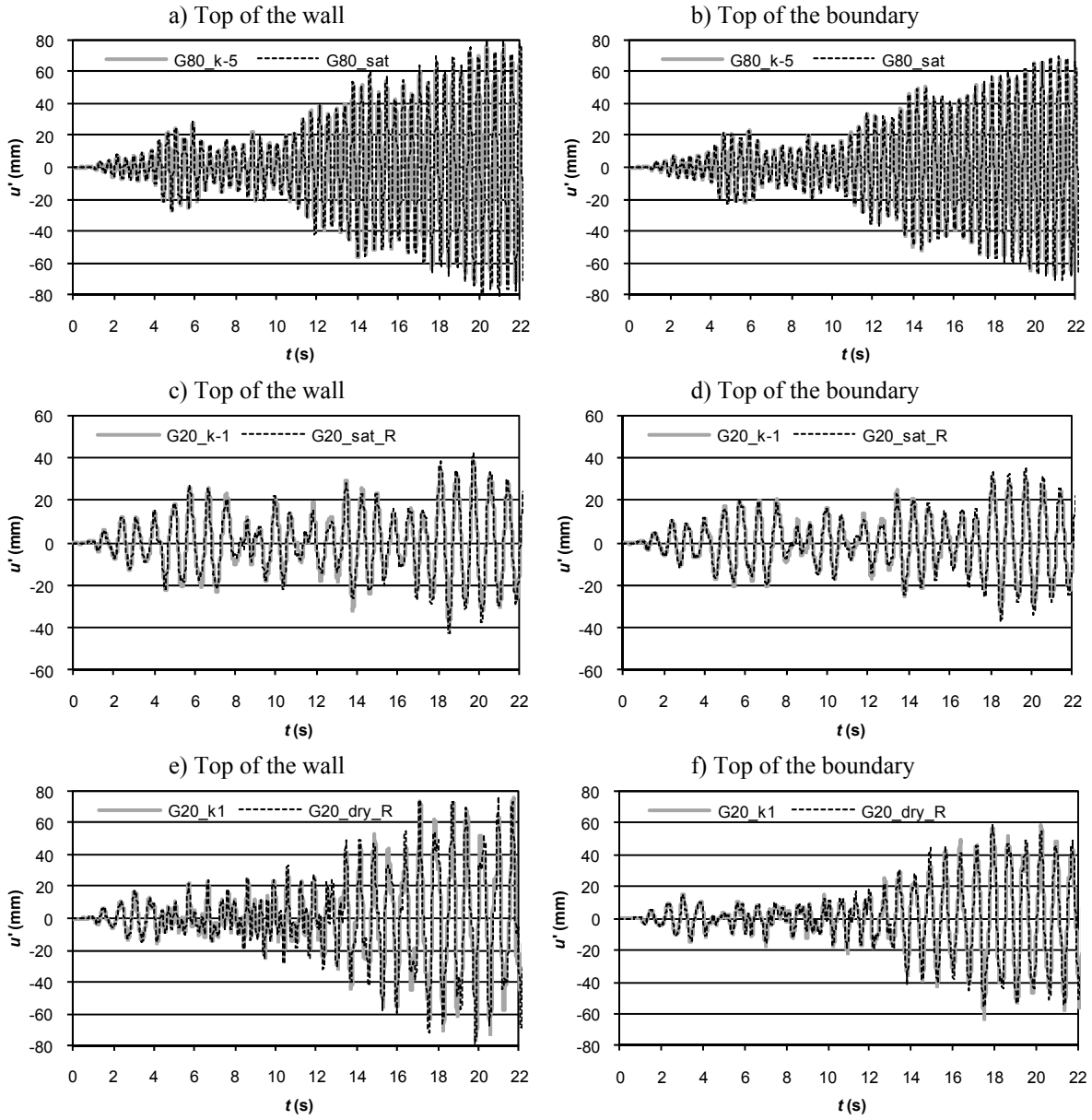

Figure 6: Time variation of displacement amplitudes for the layers with embedded wall.

The volumetric deformations, ε_v, were calculated in some control points (Fig. 1) for several depths and for distances from the wall not less then 2m. The results of the time variation of ε_v are displayed in Figure 7 for the poroelastic layers G20_k-5 and G80_k-1. For both cases, it is evident that results at the boundary points are quite different from those at the inner zone of the layer. This should be due to the slide restrictions imposed at the lateral boundaries layers.

Also, the time variation of ε_v is less uniform from point to point in the layer with higher permeability, due to the fact that for k=1×10^{-5}m/s the behaviour is more similar to the undrained case in the whole of the inner zone of the layer.

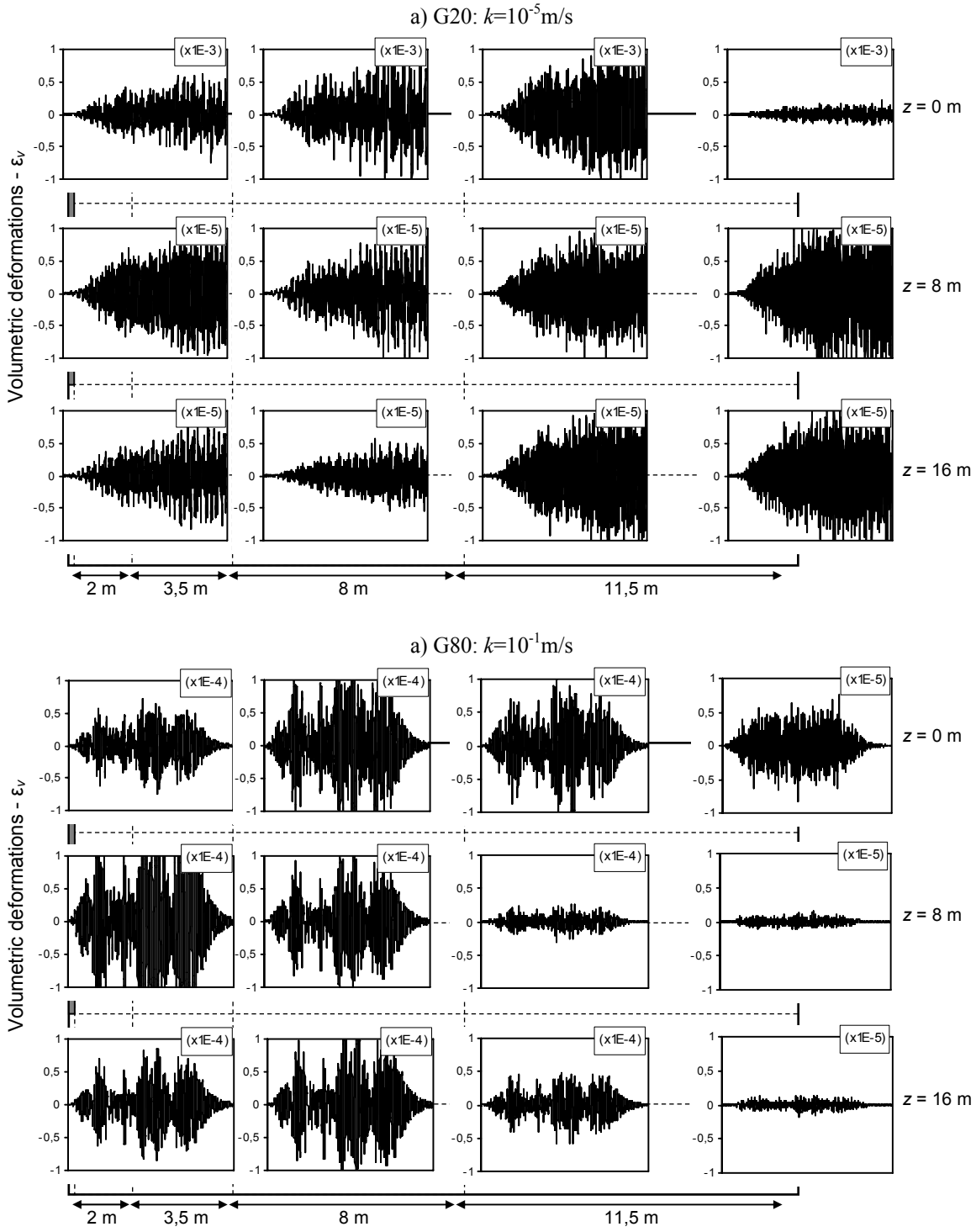

Figure 6: Volumetric deformations in layers G20_k-5 and G80_k-1 with embedded wall.

5 CONCLUSIONS

The results presented in this paper show that non-porous materials with appropriate properties and Rayleigh damping may reproduce almost perfectly pure shear behaviour of poroelastic layers. The good results obtained in the comparative analyses between both materials validate the method used for the determination of Rayleigh coefficients.

Subsequent similar analyses were made for layers with an embedded wall. In these cases, the volumetric deformations induce slight differences between responses of both materials, more noticeable for the less damped cases. Nevertheless, calculations of the responses of layers with the embedded wall reveal fairly rigorous results with non-porous materials, despite the pore fluid pressures presented in poroelastic cases. The use of non-porous materials has the aforementioned benefits in effort and time computation.

For the analyses with the embedded wall in poroelastic materials, a more uniform field of volumetric deformations is observed for permeabilities near limit coupled cases, meaning that over whole inner media has a similar behaviour.

REFERENCES

[1] Biot, M.A. Theory of propagation of elastic waves in a fluid-saturated porous solid. I. Low frequency range. *J. Acoustical Soc. of America* (1956) **28(2)**: 168-178.

[2] Biot, M.A. Theory of propagation of elastic waves in a fluid-saturated porous solid. II. Higher frequency range. *J. Acoustical Soc. of America* (1956) **28(2)**: 179-191.

[3] Schanz, M.; Diebels, S. A comparative study of Biot's theory and the linear theory of porous media for wave propagation problems*, Acta Mechanica* (2003) **161**: 213-235.

[4] Zienkiewicz, O.C.; Chang, C.T.; Bettess, P. Drained, undrained, consolidating and dynamic behaviour assumptions in soils, *Geotéchnique* (1980) **30(4)**: 385-395.

[5] Grazina, J.C.; Pinto, P.L. and Taborda, D. Evaluation of viscous damping due to solid-fluid interaction in a poroelastic layer subjected to shear dynamic actions, NUMGEO (2010), Trondheim, pp. 447-452.

[6] Grazina, J.C. Modelação dinâmica com acoplamento viscoso de maciços elastoplásticos. Aplicação a estruturas de suporte flexíveis submetidas a acções sísmicas. *PhD thesis, University of Coimbra* (in Portuguese), (2010).

[7] Zienkiewicz, O.C.; Chan, A.H.C.; Pastor, M.; Schrefler, B.A. and Shiomi, T. *Computational Geomechanics with Special Reference of Earthquake Engineering*. John Wiley & Sons, Chichester, (1999).

[8] Arduino, P. and Macari, E.J. Implementation of a porous media formulation for geomaterials. *J. Eng. Mechanics*, *ASCE*, (2001) **127(2)**, pp. 157-166.

[9] Gajo A. Influence of viscous coupling in propagation of elastic waves in saturated soil. *J. Geot. Engineering*, ASCE, (1995) **121(GT9)**, pp. 636-644.

[10] Seismosignal – "A computer program for signal processing of strong-motion data" [online]. Available from URL: http://www.seismosoft.com.

[11] Eurocode 8 – NP, EN 1998-1: Design of structures for earthquake resistance, (2010).

[12] Taborda, D. DFTi – Improved Discrete Fourier Transform Algorithm software: version 1.1.1, (2008).

[13] Kramer, S.L. *Geotechnical Earthquake Engineering*. Prentice Hall, New Jersey, (1996).